Analytica Chimica Acta 1378 (2025) 344694

Contents lists available at ScienceDirect

Analytica Chimica Acta

journal homepage: www.elsevier.com/locate/aca

Improving detection and figures of merit in single-particle inductively coupled plasma-mass spectrometry via transient event heights

Antonio Bazo [a], Lorién López-Villellas [b], Matilde Mataloni [a,c], Eduardo Bolea-Fernandez [a], Ana Rua-Ibarz [a,*], Marco Grotti [c], Maite Aramendía [a], Martín Resano [a,**]

[a] University of Zaragoza, Department of Analytical Chemistry, Aragon Institute of Engineering Research (I3A), Zaragoza, 50009, Spain
[b] University of Zaragoza, Department of Computer Science and Systems Engineering, Aragon Institute of Engineering Research (I3A), Zaragoza, 50018, Spain
[c] University of Genoa, Department of Chemistry and Industrial Chemistry, Genoa, 16146, Italy

HIGHLIGHTS

- Using peak height as the signal in SP-ICP-MS is evaluated by monitoring AuNPs.
- A new cumulative method for estimating the peak height accurately is proposed.
- Peak height correlates linearly with the square of the NP diameter.
- A new method for estimating a more reliable LoD based on peak heights is proposed.
- Peak height improves smaller NP sizing and helps in flagging incorrect thresholds.

GRAPHICAL ABSTRACT

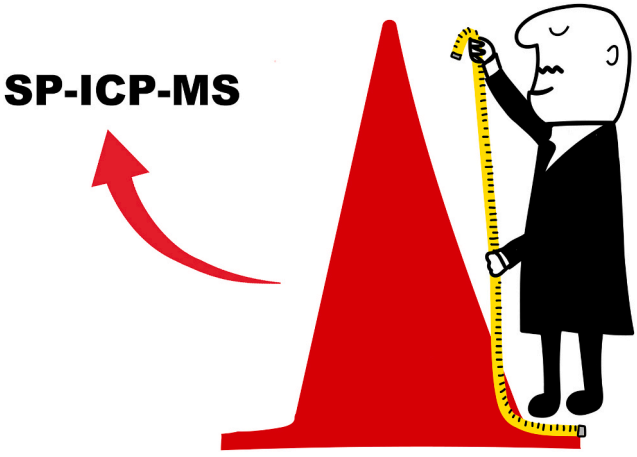

ARTICLE INFO

Handling Editor: Xiu-Ping Yan

Keywords:
Single-particle inductively coupled plasma-mass spectrometry (SP-ICP-MS)
Nanoparticles (NPs)
Limit of detection (LoD)
Peak height
Figures of merit

ABSTRACT

Background: Single-particle inductively coupled plasma-mass spectrometry (SP-ICP-MS) is a powerful method for characterizing micro- and nanoparticulate materials. The technique primarily relies on the linear relationship between the integrated intensities of individual events (peak areas) and the analyte mass, though transit times (peak widths) have also been used for quantitative purposes. This work (1) evaluates the potential of using peak heights as analytical signals in SP-ICP-MS, (2) introduces a new method for determining peak heights, and (3) explores scenarios in which peak height offers added value over the commonly used SP-ICP-MS signals.
Results: A new method was proposed to estimate peak height values in SP-ICP-MS accurately. The cumulative intensity across consecutive dwell times was modeled using a third-degree polynomial, from which the adjusted peak height was derived. This approach reduces the uncertainty associated with using raw maximum intensity values, yielding NP distributions comparable to those obtained via integrated intensities. The effect of dwell time

* Corresponding author.
** Corresponding author.
E-mail addresses: arua@unizar.es (A. Rua-Ibarz), mresano@unizar.es (M. Resano).

https://doi.org/10.1016/j.aca.2025.344694
Received 9 July 2025; Received in revised form 10 September 2025; Accepted 22 September 2025
Available online 22 September 2025

on peak height was also evaluated. An optimal range (50 μs–200 μs) was identified, where a linear relationship was observed between the peak height and the square of the NP diameter. Within this range, peak height showed the lowest bias when characterizing smaller NPs, indicating the potential to improve the limit of quantification (LoQ). Additionally, peak heights proved helpful in determining the limit of detection (LoD) and setting appropriate threshold values for data processing, thereby helping to flag incorrect resultsand addressing a challenge in SP-ICP-MS analysis.

Significance: This is the first study to evaluate peak height as an analytical signal in SP-ICP-MS. The results highlight its advantages in specific applications, such as sizing NPs near the LoD, and in supporting the more reliable use of other signals, such as peak areas, by helping to identify incorrect threshold selection that could lead to biased distributions. Finally, monitoring peak heights allows for a more realistic and assumption-free determination of the LoD.

1. Introduction

As a result of their unique size-dependent properties that distinguish them from their larger-scale (bulk) counterparts, nanoparticles (NPs) have emerged as a critical component in a wide range of industrial, environmental [1–3], food [4–6], and biomedical applications [7,8]. The growing production and use of NPs necessitates the development of accurate, sensitive, and reliable methods for their appropriate characterization. Among other techniques, single-particle inductively coupled plasma-mass spectrometry (SP-ICP-MS) has become a technique of growing interest given its potential to provide comprehensive information on mass and size distributions, as well as particle number concentration (PNC), of NPs in real samples with minimal preparation [9,10]. In SP mode, NPs that are effectively transported into the ICP ion source are vaporized, atomized, and ionized in the plasma, resulting in very short transient ion signals (single events).

Following the seminal paper by Degueldre et al. introducing the SP-ICP-MS technique in 2003 [11], several data treatment strategies have been proposed to handle the fast, temporally resolved signals generated by SP-ICP-MS measurements [12–15]. The integrated intensities (areas) of the individual events have been predominantly used in most studies, as this analytical signal was found to be proportional to the NP mass. Subsequently, the mass could be used to determine the NP size, assuming a well-known shape, density, and chemical composition [10, 16].

It is important to recognize that in the early years of SP-ICP-MS, the ICP-MS instrumentation was limited to dwell times in the millisecond range, so every individual event was characterized by a single data point and, therefore, there was no choice on what signal parameter should be used for quantification. However, instrumental developments enabled the use of ultrafast data acquisition speeds, with dwell times down to the micro- and even nano-second range [17,18]. In principle, this allows for the accurate monitoring of the transit time (width) of the events [19,20], which, in contrast to the peak area, is directly proportional to the NP size. The use of the transit time significantly simplifies the calculations and, far from assuming NP sphericity, it provides some nano-morphological information [21]. However, this approach has been applied only occasionally and is still not widely adopted, which can be attributed to the difficulties associated with accurately identifying the temporal boundaries of the events, given that they are not recorded continuously but rather through successive dwell times during which the instrument accumulates signal intensity [22].

The use of dwell times in the microsecond range also enables the selection of the peak height as the analytical signal in SP-ICP-MS, but this possibility has been overlooked in this context so far. However, the need to evaluate transient signals is by no means exclusive to this technique. Other techniques, such as chromatographic approaches or graphite furnace-based techniques, to name just two mature ones, produce time-resolved peak signal outputs. For these techniques, all possible strategies to obtain quantitative information (peak areas, peak widths, but also peak heights) have been investigated, all of them showing specific advantages. For instance, peak height is less affected by the partial overlap of consecutive events than peak area [23–25], and it can also provide greater accuracy when the signal-to-noise ratio (S/N) is low [26]. Obviously, the use of peak height also shows some disadvantages. Specifically, it may be less representative of the analyte content than the peak area when the mechanism of signal formation for the sample and the calibration standard differs.

Returning to SP-ICP-MS, it is important to realize that the peak height is already the parameter of choice for setting the threshold above which the intensity spikes are considered to correspond to an NP. The current data processing SP-ICP-MS software programs rely on the selection of critical integration limits (I_c) to distinguish between those intensity peaks originating from suspended NPs and those stemming from the continuum background (BG) [20,27–29]. Therefore, any intensity event with a maximum exceeding this threshold is considered part of the NP distribution, whereas those below the limit are used for background correction. The selection of this critical value is of major importance to avoid misestimating both the number of detected events (related to the PNC) and the intensity distribution (which affects the determined particle size). In other words, height-based criteria are relied upon for the identification of NP events and the subsequent determination of peak areas.

Additionally, this threshold is used for calculating the limit of detection (LoD), but several assumptions are required to correlate the height-based criterion with its corresponding area [30]. Consequently, the monitoring of the peak heights could not only withdraw such assumptions but also simplify the calculations, as no conversion between analytical signals is required. It is therefore surprising that, to the best of the authors' knowledge, the potential of peak height as an analytical signal for quantitative purposes has not yet been explored in SP-ICP-MS, especially given the relative ease of identifying the maximum intensity (height) compared to the integrated intensity (area) or temporal boundaries (width).

In this work, the potential use of peak heights as analytical signals in SP-ICP-MS has been evaluated for the first time. Using AuNPs as a model, data acquisition parameters and data processing methods have been optimized for the simultaneous determination of the integrated intensity (area), transit time (width), and maximum intensity (heights) of the detected events. The performance of all three analytical signals has been assessed for characterizing AuNPs across a wide mass range (0.1–9.9 fg). The SP-ICP-MS results obtained using the different strategies have been compared with each other and with the reference values provided by the manufacturer, allowing for conclusions to be drawn on the selection of the preferred signal quantification strategy in various analytical situations.

2. Materials and methods

2.1. Reagents, standards, and samples

Analytical purity grade reagents were used throughout this work. Ultra-pure water (resistivity >18.2 MΩ cm) was obtained from a Milli-Q water purification system (Millipore, France).

All experiments were conducted by analyzing aqueous suspensions of highly monodisperse (Ultra Uniform™) AuNPs with nominal

diameters of 10 (9.6 ± 0.4 nm), 20 (20.8 ± 0.5 nm), 30 (28.2 ± 0.6 nm), 50 (51.0 ± 1.9 nm), and 100 nm (99.4 ± 3.1 nm) (Nanocomposix Europe, Czech Republic). All NP suspensions were appropriately diluted with ultra-pure water until a PNC of approximately 5×10^4 NPs mL^{-1}, so that the probability of facing double events was kept below 0.1 %.

For quantitative SP-ICP-MS analysis (size determination), external calibration was performed by establishing linear correlations between the analytical signals and NP-specific properties: integrated intensity vs. NP mass ($\propto d^3$), signal width vs. NP diameter ($\propto d$), and signal height vs. the square of the NP diameter ($\propto d^2$). The specific NP property to which the signal is linearly proportional is described in detail below.

2.2. Instrumentation

All measurements were carried out using a NexION 5000 (PerkinElmer, USA) ICP-MS/MS instrument. The sample introduction system comprised a concentric quartz nebulizer (0.4 mL min^{-1}) and a quartz cyclonic-type spray chamber. The triple cone interface with OmniRing™ was operated in extraction mode to achieve maximum sensitivity. The instrument is equipped with a quadrupole ion deflector (QID, Q0) that selectively focuses the ion beam over a 90-degree angle, prior to its introduction into the mass spectrometer (MS). The MS consists of two additional quadrupole mass analyzers (Q1 and Q3) and a quadrupole collision/reaction cell (CRC; Q2) located in between. In this work, the instrument was operated in single-quadrupole or "Q3 Only" mode, so that the first full-sized resolving quadrupole (Q1) was fully open. The CRC was pressurized with an optimized NH_3 gas flow rate (0.45 mL min^{-1}) and operated in Reaction mode. This mode enhances sensitivity compared to the non-Reaction mode, due to a collisional focusing effect. For SP-ICP-MS analysis and preliminary data visualization, the instrument is equipped with the Syngystix Nano Application module (v3.5).

Daily performance checks were carried out to ensure optimum instrument performance. The torch position, QID, and gas settings were optimized accordingly to achieve maximum sensitivity for Au while maintaining the $Ce^{++}(70)/Ce^{+}(140)$ and $CeO^{+}(156)/Ce^{+}(140)$ ratios equal to or under 0.03 and 0.025, respectively. Instrument settings and data acquisition parameters are summarized in Table 1.

2.3. Data processing

To process the data exported from the Syngystix Nano Application module, a previously developed in-house Phyton script was modified, using the scipy. optimize library for polynomial fittings and derivatizations to provide all three analytical signals of interest: peak area, peak width, and peak height [20]. For further details on determining peak heights, readers are referred to the corresponding discussions in section 3. The processed datasets were fitted to Gaussian distributions to calculate their central values using the OriginPro software (version 2021b, 9.85 OriginLab Corporation, USA), which was also used for plotting, interpolation, and statistical analysis throughout the study.

Table 1
Instrument settings and data acquisition parameters for the NexION 5000 ICP-MS/MS instrument.

Measurement conditions	
RF Power, W	1600
Nebulizer gas flow, L min^{-1}	1.01
Plasma gas flow, L min^{-1}	16
Auxiliary gas flow, L min^{-1}	1.2
Detection mode	Q3 Only
Q3 mass, amu	197
Dwell time, μs	10–3000
Acquisition time, s	60
Reaction mode	0.45 mL min^{-1} NH_3
RPq	0.25
QID, V	−9.0
Instrumental setup	
Spray chamber	Quartz cyclonic spray chamber
Nebulizer	Type A concentric nebulizer
Introduction system	Peristaltic pump
Uptake rate, mL min^{-1}	0.4
NP parameters for calculations	
AuNP density, g cm^{-3}	19.32

3. Results and discussion

3.1. Determination of the peak height

To evaluate the potential of using the maximum signal intensity (peak height) as an alternative analytical signal to the integrated intensity (peak area) and transit time (peak width) in SP-ICP-MS, AuNPs across a wide mass range (0.1–9.9 fg) were analyzed. For appropriate assessment, it was first necessary to modify a previously developed data processing script [20]. This new home-made script version allows for the simultaneous calculation of the peak height, peak area, and peak width of each individual event, thus allowing for a fair comparison of the SP-ICP-MS results [20].

A priori, heights can easily be determined as the maximum signal intensity reading registered for each individual event detected. Ideally, continuous monitoring would correspond to an infinitesimally short dwell time, effectively enabling real-time, uninterrupted signal detection. However, ICP-MS detection accumulates signal over discrete, user-defined dwell times, resulting in a temporally averaged measurement rather than a truly continuous intensity trace. In other words, if the duration of a transient event is longer than a single dwell time, its signal is distributed across multiple adjacent readings. The use of relatively long dwell times jeopardizes the accuracy with which heights can be determined, as the very same event can lead to different maximum intensities (I_{MAX}) depending on how the signal intensities corresponding to the NP ion cloud are fractioned within the time window, as represented in Fig. 1A–D. This new source of imprecision, caused by the fractioning of events into multiple data points, where the number of data points depends on both the event duration and the selected dwell time, results in the broadening of the recorded distribution compared to that of the integrated intensities (peak areas), as can be seen in Fig. 1E and F.

To circumvent this issue, this work proposes a new strategy to determine the peak height in SP-ICP-MS. This approach is based on the representation of the evolution of the cumulative intensity (the sum of the individual signals of the events; y-axis) versus the readings (consecutive dwell times; x-axis), as illustrated in Fig. 1G and H. The cumulative intensity corresponds to the integrated intensity (area), and is thus proportional to the NP mass and, consequently, to the cube of the NP diameter (d_{NP}^3). The number of readings is a measurement of the peak width, and is therefore proportional to the NP diameter (d_{NP}) [19–21]. As a result, the evolution can be adjusted to a third-degree polynomial function ($R^2 = 0.99 \pm 0.01$), from which the adjusted height is calculated as the point where the first derivative reaches its maximum (δ_{MAX}). The use of this approach minimizes the effect of event fragmentation and, therefore, the widening of the overall NP distributions (Fig. 1I). As an illustrative example, the difference in peak height of the two events of equal peak area, and therefore mass, represented in Fig. 1, was reduced from values of 52 (Figs. 1C) and 68 counts (Fig. 1D) for I_{MAX} to values of 44 and 47 counts, respectively, for δ_{MAX}.

The new approach clearly minimizes the source of imprecision in the determination of the peak height and significantly overcomes the broadening of the peak height distributions as compared to those relying on the peak areas (as can be observed by comparing Fig. 1E and I). Still, the distributions tend to exhibit some degree of asymmetry in the form of positive tails, which can probably be attributed to NPs whose ion clouds expanded less and led to abnormally short and highly intense events [21,31].

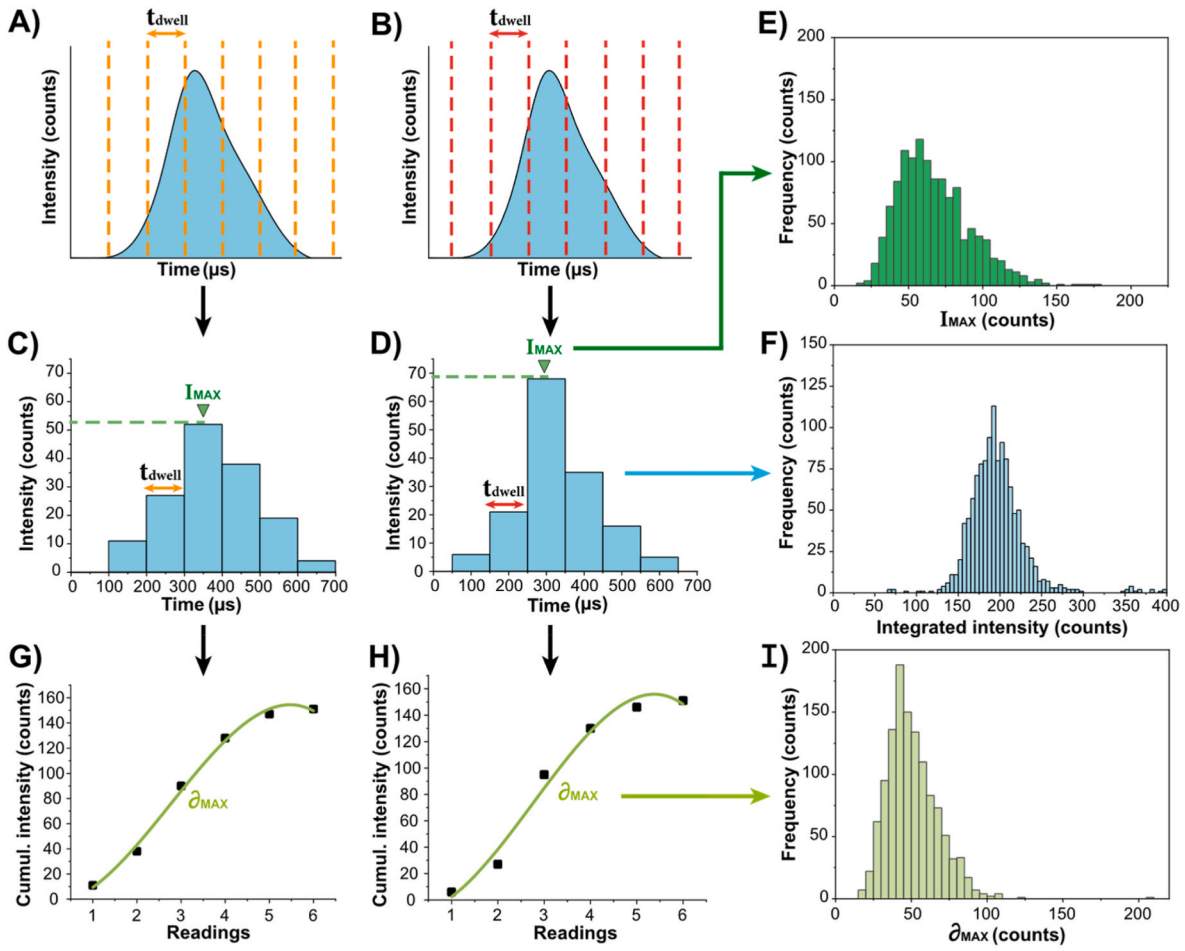

Fig. 1. Scheme illustrating the data processing of two events with identical integrated intensity (A,B), but differing in how the total intensity signal is distributed across dwell times (C,D). From these, the maximum and integrated intensities are used to derive the NP height (E) and area (F) distributions, respectively. Each event is then fitted with a third-degree polynomial function, from which the maximum first derivative (δ_{MAX}) is extracted (G,H) to calculate the corrected height distribution (I).

It is also relevant to clarify that for smaller NPs, where the limited number of detectable readings may be insufficient to fit a third-degree polynomial function, as will be shown in section 3.3., the maximum intensity can still be used as predictor of the peak height.

3.2. *Effect of dwell time on the peak height*

In addition to the data processing, selecting an adequate dwell time has also been reported to significantly impact the accuracy and precision with which both peak areas and peak widths are determined [20]. To assess the effect of the dwell time on the peak height determination compared to the other analytical signals, all the available AuNP suspensions were analyzed in quintuplicate at different dwell times: 10, 20, 50, 100, 200, 500, 1000, and 3000 µs. Fig. 2 shows the results obtained for the 50 nm AuNPs, which were similar to those obtained for other NP sizes. As can be seen, the same average peak area was registered for all the dwell times within the 50–3000 µs dwell time range. However, the average intensity starts to decrease for the low dwell time values, as some of the readings fall under the limit of detection (LoD). In contrast, the determined average peak width was found to be stable for dwell times under 200 µs only, whereas for higher values, due to the lack of sufficient temporal resolution, all the intensity starts to be accumulated within a single reading until, eventually, the determined peak width matches the dwell time. As to the average peak height, the intensity increases proportionally with the dwell time, as more ions are detected during each reading. However, similarly to the peak width, the signal starts to be registered within a single reading for dwell times above 200 µs and, thus, the peak heights asymptotically tend to the peak area. In conclusion, peak height measurements must be determined within the range of dwell times where the peak width remains stable, and all three analytical signals can be precisely determined within the 50–200 µs range for the 50 nm AuNPs. Nevertheless, it is worth mentioning that this dwell time range is shortened for smaller NPs (50 µs for 20 nm AuNPs, 50–100 µs for 30 nm, and 50–200 µs for 100 nm AuNPs), as they render lower transit times. Therefore, 50 µs was selected as the dwell time for implementing the proposed approach, as it was found suitable for every NP size.

3.3. *Impact of analytical signal type on the linear response*

After developing a suitable approach for determining the event heights and selecting an appropriate dwell time for further evaluation, the linear response range was evaluated for the three analytical signals: peak area, peak width, and peak height. For this purpose, all four monodisperse AuNP standards and a blank solution (ultra-pure water) were analyzed in quintuplicate, and their corresponding average values were used to construct the calibration curves displayed in Fig. 3. Subsequently, the experimental sizes (d_{exp}) were determined by interpolating each analytical signal in its corresponding curve. The results were compared to those provided by the manufacturer (reference value; d_{ref}) in the certificate of analysis of the standards, according to Eq. (1).

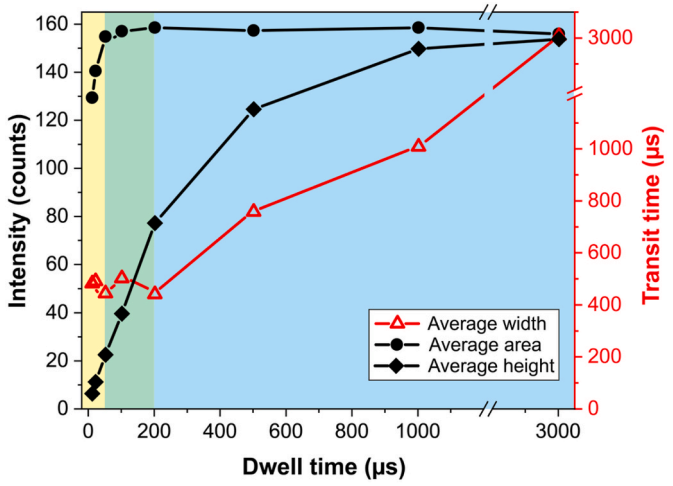

Fig. 2. Effect of the dwell time on the determined average peak area, peak width, and peak height of a 50 nm AuNP suspension (n = 5). Uncertainties expressed as standard deviations are included but overshadowed by the data-points. The region shaded in yellow and green (≤200 µs) represents the optimum dwell times for the monitoring of both peak widths and peak heights, whereas the optimum range for the determination of the peak areas is highlighted in green and blue (≥50 µs). The green colored region (50–200 µs) is the result of combining yellow and blue, and it represents the dwell time range for which all three analytical signals can be precisely calculated. (For interpretation of the references to color in this figure legend, the reader is referred to the Web version of this article.)

$$\text{Bias}\ (\%) = \frac{|d_{exp} - d_{ref}|}{d_{ref}} 100 \quad (1)$$

A good linearity ($R^2 = 0.99993$) was obtained when using the peak area as the analytical signal, as shown in Fig. 3A. However, significant deviations from the calibration curve were observed for the 20 nm and 30 nm NPs, resulting in biases of 14.9 % and 4.9 % respectively. In the case of the peak width measurements, the relationship remained linear until the point corresponding to the 50 nm AuNPs, beyond which the use of the peak width no longer followed a linear trend, as can be seen for the 100 nm AuNPs (Fig. 3B).

The observation of abnormally short transit times for the larger NPs was previously reported in an earlier study [20]. This was attributed to particle digestion occurring further downstream in the plasma (*i.e.*, closer to the sampling cone), where diffusion and mixing processes responsible for the expansion of the ion cloud are less effective compared to those affecting smaller NPs [20]. Consequently, the 100 nm AuNPs were not included for the construction of the peak width-based calibration curve.

As to the accuracy for size determination, larger biases were observed again for the two smaller NPs (17.9 % and 17.4 % for the 20 nm and 30 nm AuNPs, respectively). Nevertheless, the difference with the 50 nm AuNPs was not significant, given the high level of imprecision inherent to the determination of the transit time, which was also responsible for the relatively poor linearity obtained for the peak width-based method ($R^2 = 0.986$).

Finally, the performance of the peak height as the analytical signal in SP-ICP-MS was evaluated. As previously indicated, the peak height intensities were found to be proportional to the squared NP diameter (d_{NP}^2), which is a parameter related to the NP surface area. This observation can be understood by the dimensional analysis of the three types of analytical signals. In this regard, the peak area and peak width are known to be proportional to the d_{NP}^3 (particle mass) and d_{NP} (particle size), respectively. Therefore, provided that the peak area is proportional to the product of the other two analytical signals (peak width and peak height) [30], peak heights need to be a function of d_{NP}^2 to guarantee

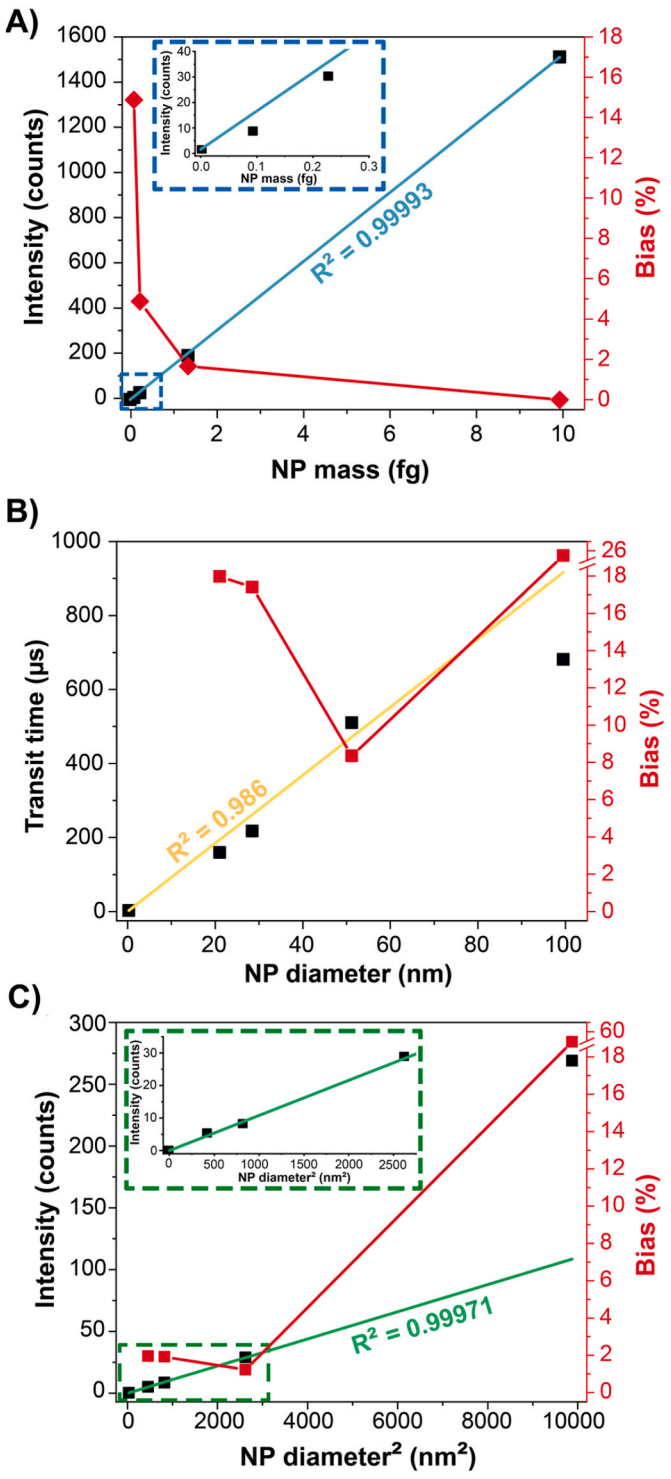

Fig. 3. Calibration curves (left y-axis) obtained with four different NP suspensions (20 nm, 30 nm, 50 nm, and 100 nm AuNPs) and a blank solution (ultra-pure water), using the peak area (A), peak width (B), and peak height (C) as analytical signals. Moreover, the bias observed when interpolating each different signal in its corresponding calibration curve is reported (right y-axis).

dimensional homogeneity. Regarding the figures of merit for calibration using the peak height, the linear response range does not include the 100 nm AuNPs because, as previously discussed, this analytical signal requires both the peak area and peak width to be proportional to d_{NP}^3 and d_{NP}, respectively. Consequently, since the peak width no longer followed a linear trend for the 100 nm AuNPs – while the peak area, virtually

unaffected by the mixing and diffusion processes experienced by the ion cloud, still did – the peak height was found to be abnormally high for the larger AuNPs (Fig. 3C), likely as compensatory effect for the narrowing of the events. The linearity for the rest of the datapoints (excluding the 100 nm AuNP) was comparable to that of the peak areas ($R^2 = 0.99971$). Importantly, no deviation from the adjusted linear fitting was found for the smaller entities, with biases of only 1.9 % for both the 20 nm and 30 nm AuNPs.

Therefore, the peak heights offer greater accuracy for the processing of SP-ICP-MS intensity peaks from small NPs characterized by a low S/N ratio. This finding aligns well with observations made using other analytical techniques, such as chromatography [26]. In the case of SP-ICP-MS analysis, a precise determination of both the peak area and peak width requires all the intensity readings triggered by the NP detection to be accounted for, while accurate determination of the peak height only requires the maximum intensity reading to be detected over the threshold above which signals are considered to belong to NPs (I_c). This different situation is illustrated in Fig. 4, in which two events registered for a 30 nm and a 20 nm AuNP are represented. As can be seen, all the readings are above I_c for the 30 nm AuNP (Fig. 4A), allowing for the accurate determination of all three analytical signals. However, for the 20 nm AuNP event (Fig. 4B), the relatively poor S/N ratio causes some readings to appear below I_c. In this case, more than 50 % of the event readings are excluded from the determination of the peak area or peak width, but this does not affect the identification of the peak height, allowing for the accurate characterization of small NPs that are closer to the LoD.

Similarly, the S/N ratio can be worsened when NPs are in the presence of the analyte in ionic form, as is often the case for real samples. To evaluate the performance of the peak heights in comparison to the other analytical signals for these analyses, the NP standards were spiked with an ionic Au solution until concentrations of 1 (BG of 7.3 ± 2.8 counts) and 2 μg L^{-1} (BG of 14.5 ± 4.3 counts) were achieved. These suspensions were then analyzed in quintuplicate, and the determined analytical signals were interpolated in their corresponding calibration curve, obtaining the experimental particle sizes collected in Fig. 5. Results ratify the improved performance of peak heights for processing low S/N events, observing smaller deviations from the reference values than for the alternative analytical signals when in the presence of 1 μg L^{-1} ionic Au for the 20 (Fig. 5A) and 30 nm AuNPs (Fig. 5B). However, when the BG is further increased (2 μg L^{-1} of ionic Au), the noise is too high for the proper identification and processing of the events, leading to biased results regardless of the analytical signal of choice. For these cases, there is always the option to further dilute the sample (as long as it is concentrated enough) and increase the time of analysis, mitigating the impact of the background. Finally, it should be noted that the ionic content affected the results for the 50 nm AuNP standard much less (Fig. 5C), given that their events were in all cases well-resolved from the BG.

3.4. Peak heights for flagging incorrect integration thresholds

Selecting an appropriate peak identification threshold is crucial for SP-ICP-MS analysis. However, there is currently no consensus on the optimal strategy, with thresholds ranging from 3σ to 8σ based on the baseline noise [29,30,32]. Furthermore, no clear indicator exists to assess the adequacy of a chosen threshold, as its impact on the peak area distribution is not always obvious. This is partly because peak-height criteria are typically used to identify true NP events when determining peak areas. To exemplify the impact of the threshold value (I_c) on both the peak area and peak height, Fig. 6A shows a representative fragment of the real-time analysis of 30 nm AuNPs with three potential critical values: 2.0 (5σ criterion), 3.0 (8σ criterion), and 6.0 counts (maximum baseline reading).

The application of three different peak identification thresholds yields three distinct peak area (Fig. 6B–D) and peak height (Fig. 6E–G)

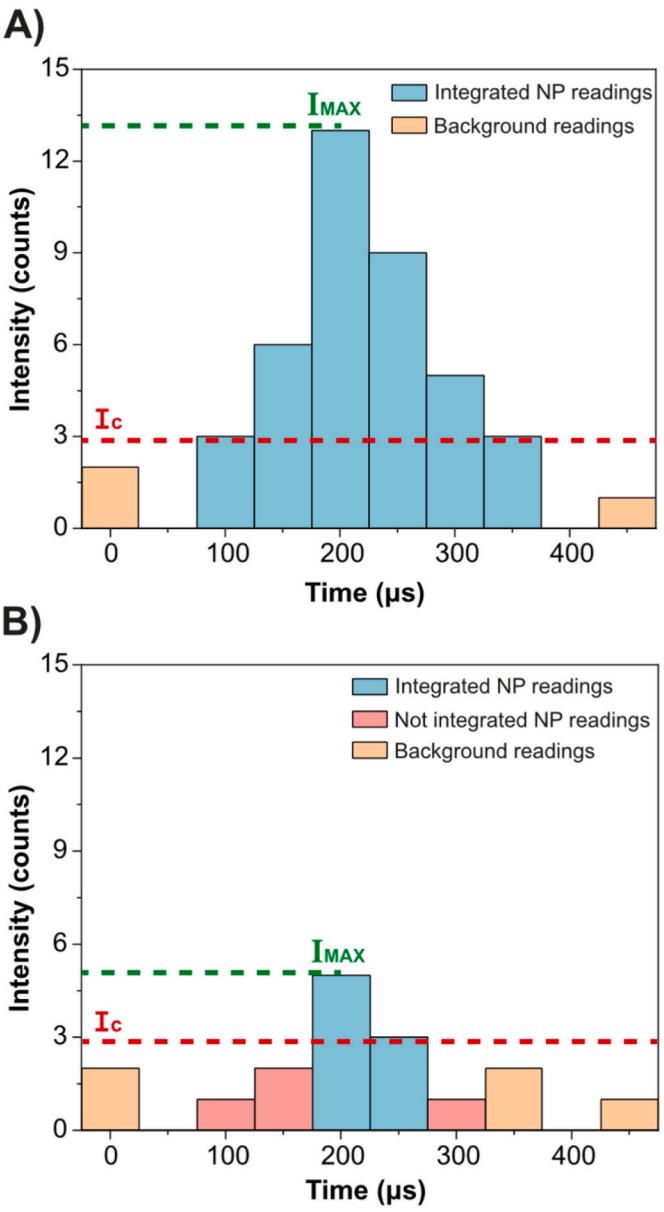

Fig. 4. Signal intensity readings monitored for a 30 nm AuNP event (A) and a 20 nm AuNP event (B). The green dashed line indicates the maximum intensity, while the red dashed line represents I_c (set with an 8σ criterion, as discussed in Section 3.4). Data points associated with the NP are shown in blue when above I_c, and in red when below it. Orange data points represent background signals and are, a priori, not related to the NP event. (For interpretation of the references to color in this figure legend, the reader is referred to the Web version of this article.)

distributions. An a priori optimum critical value ($I_c = 3.0$ counts) results in the detection of 789 events, with both the peak area (Fig. 6C) and peak height (Fig. 6F) distributions showing well-defined Gaussian-like fits centered at 27.4 and 8.8 counts, respectively. A reduction of the threshold value ($I_c = 2.0$ counts) results in an increase in the number of detected events (1305), which can be attributed to the counting of background spikes.

In this specific case, provided that the true NP distributions are known to be Gaussian and fully resolved, it is straightforward to identify and discard the background signals (Fig. 6B–E), thereby avoiding their impact on the determined PNC. However, this data purification approach lacks feasibility for complex samples with high concentrations of the analyte in ionic form, or when there is no previous information on

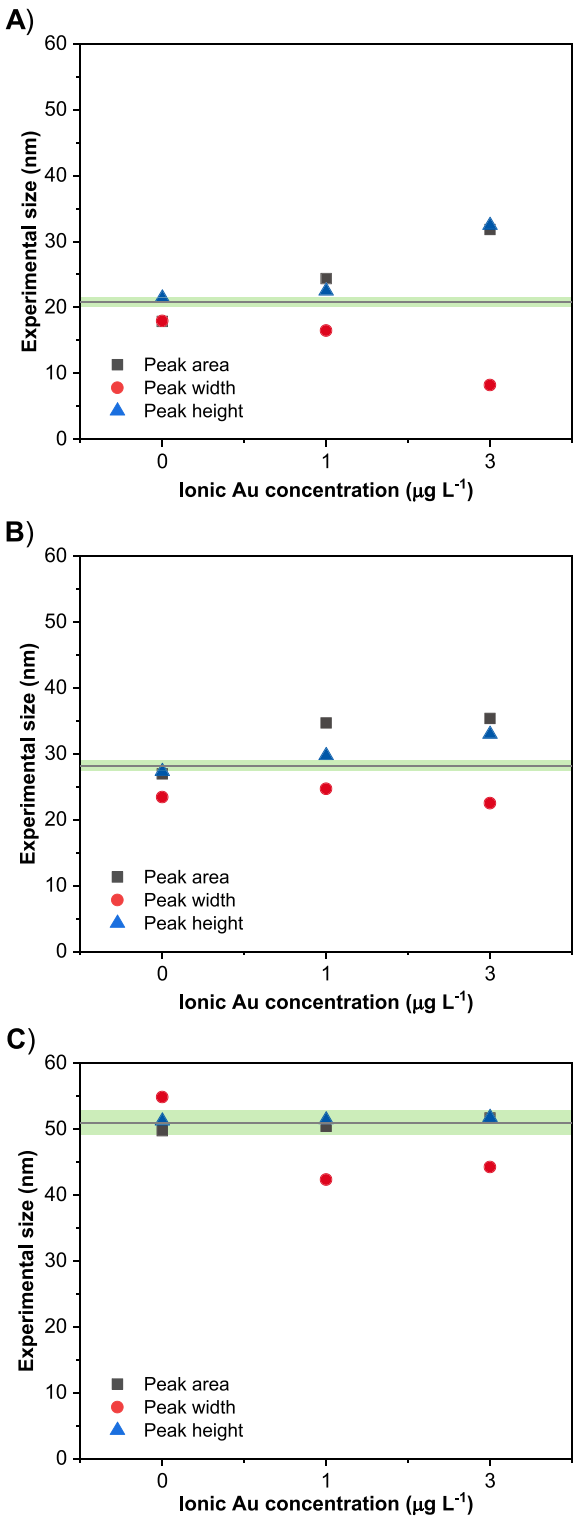

Fig. 5. Experimental sizes determined for the 20 (A), 30 (B), and 50 (C) AuNP standards in the presence of different ionic Au concentrations, using the different analytical signals. The reference range of sizes provided by the manufacturer is shaded in green. The error bars represent the standard deviation (n = 5). Some error bars in (C) are smaller than the symbols and, thus, cannot be appreciated. (For interpretation of the references to color in this figure legend, the reader is referred to the Web version of this article.)

the shape of the NP distribution. Additionally, data processing scripts use the intensity readings that are not identified as belonging to any NP to subtract the baseline contribution from the true event signals. Therefore, when the critical value is too low, the most intense background readings are not averaged for noise correction, as they are considered to be part of the NP distribution, leading to biases in the NP signal distribution due to the underestimation of the baseline contribution.

It should be noted that peak areas are more affected by this issue than peak heights, as the former involves the contribution of multiple readings. Accordingly, whereas the peak area distribution curve is slightly biased high and centered at approximately 28.0 counts (Fig. 6B), the peak height distribution remains unaffected and centered at 8.8 counts (Fig. 6E).

Finally, for the higher threshold value (I_c = 6.0 counts), the number of registered events was reduced to 697, which would result in a 12 % underestimation of the PNC. Surprisingly, the shape of the peak area distribution was barely affected by the selected threshold (Fig. 6D), while that of the peak heights was clearly incomplete (Fig. 6G). The reason behind this observation is that, as previously mentioned, the threshold value relies on a height-based criterion, so that the distributions only show those events with heights above the new threshold, leading to incomplete height histograms when the critical value divides the NP distribution. However, this is not the case for the peak areas because high-intensity events do not necessarily entail higher peak areas, since this also depends on the peak width. Therefore, regardless of the selected threshold, the peak area distribution always shows an apparent complete curve that is slightly shifted to higher intensities (27.7 counts in the case represented), which could lead to the deceptive conclusion that the threshold value is well selected.

Based on these results, peak height distributions can be used not only for direct quantification but also as a promising tool to evaluate the appropriate selection of the threshold value, thus supporting the effective use of peak areas in quantitative SP-ICP-MS analysis.

This addresses an important issue for SP-ICP-MS, and for single-event ICP-MS in general, a field in which it is not simple to validate the results of the distribution obtained, as different techniques may offer variations in this regard [33]. Therefore, it becomes essential to have tools that can flag incorrect results.

3.5. Peak heights for the accurate determination of the LoD

The determination of the LoD in SP-ICP-MS (*i.e.,* the minimum detectable NP size) remains challenging nowadays, as there is no fully established strategy for its estimation. In principle, an NP can be detected as long as one of its triggered readings is more intense than the integration threshold I_c. However, the challenge lies in the correlation of such a signal with its corresponding particle size, since, as previously discussed, most of the readings are undetected when the maximum intensity of an NP is close to I_c. Therefore, to determine the LoD, it seems necessary to estimate the area of an event with peak height equal to I_c for its interpolation in the peak area calibration curve.

For this purpose, Laborda et al. [30] proposed the approximation of the NP events to triangles so that their theoretical areas can be geometrically calculated as a function of their height (I_c), width (w) and the dwell time (t_{dwell}), after correcting for the contribution of the average intensity of the BG (I_{BG}). Then, this calculated area can be interpolated in a peak area calibration curve of sensitivity K_{area} for the determination of the minimum detectable NP mass (LoD_{mass}), according to Eq. (2).

$$LoD_{mass} = \frac{(I_c - I_{BG})\, w}{2\, t_{dwell}\, k_{area}} \quad (2)$$

Similarly, the minimum detectable size (LoD_{size}) can be obtained by assuming NP sphericity and as a function of its density (ρ), in accordance

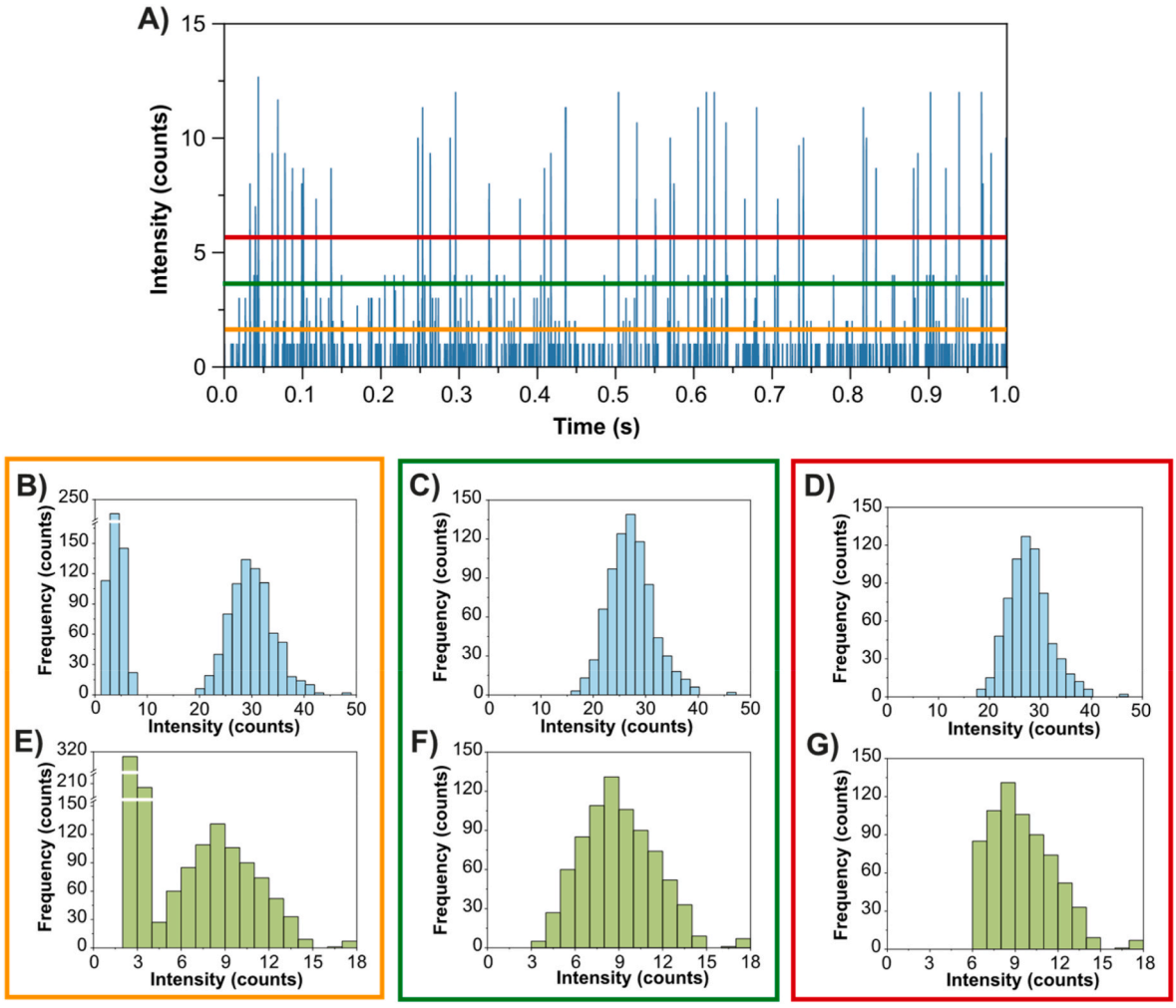

Fig. 6. Signal output of a 30 nm AuNP suspension when selecting three different threshold values (A), resulting in three different peak area (B–D) and peak height (*E*–G) distributions for the low, optimum, and high critical values, respectively.

with Eq. (3).

$$LoD_{size} = \sqrt[3]{\frac{3\,(I_c - I_{BG})\,w}{t_{dwell}\,k_{area}\,\pi\,\rho}} \quad (3)$$

This approach can be considered the most widely used today, and it is certainly useful to compare different SP-ICP-MS methods. However, it is limited by the necessity of assuming triangular peak profiles. Also, estimating the peak width results in an additional source of imprecision, given the limitations inherent to the estimation of the transit times [20]. As a result, in our experience, it tends to overestimate the detection power of SP-ICP-MS.

To circumvent all these issues, this work proposes the direct interpolation of the BG-corrected integration threshold (I_c- I_{BG}) in a peak height calibration curve of sensitivity k_{height} so that the LoD_{size} can be calculated as the square root of the resulting value, according with Eq. (4). This approach is only possible provided that, as previously discussed, the detection criterion in SP-ICP-MS is based on heights, leading to a new strategy that is not only more straightforward, but also more accurate and free from assumptions, for the determination of the LoD.

$$LoD_{size} = \sqrt{\frac{(I_c - I_{BG})}{k_{height}}} \quad (4)$$

In this work, the LoD_{size} determined with this new, peak height-based approach for AuNPs was calculated to be 16.6 nm, whereas the precedent strategy discussed above [30] underestimated the LoD down to 9.9 nm. According to the peak height calibration, this latter particle size would in reality correspond to a peak height of only 1.07 counts, which is clearly under I_c. Moreover, to validate the accuracy of the new method, a suspension of 10 nm AuNPs was introduced in the system, and no event was found over the integration threshold under our working conditions, while as shown in section 3.3., 20 nm AuNPs can be clearly detected. Consequently, we believe that monitoring peak heights offers a more realistic approach to estimating the true detection power in SP-ICP-MS.

4. Conclusions

In this work, the potential of using peak height as an analytical signal in SP-ICP-MS measurements was evaluated for the first time. Its performance was compared with that of peak area (most widely used nowadays) and peak width. Direct determination of peak height (maximum signal) provides a straightforward approach for processing complex SP-ICP-MS datasets. However, the signal accumulation over user-defined dwell times introduces uncertainty that broadens the NP size distributions. To address this, a new method was proposed that represents cumulative intensity across consecutive dwell times using a third-degree polynomial, so the adjusted peak height is determined as its maximum derivative, reducing the uncertainty and producing narrow NP distributions, comparable to those obtained via integrated intensities. The effect of dwell time on peak height determination was also

evaluated. The optimal value was established to be 50 μs, as commonly used in current SP-ICP-MS methods.

Linear relationships were observed for all three analytical signals: integrated intensity correlated to the cube of NP diameter (NP mass), peak width with NP diameter, and peak height with the square of the NP diameter. Although peak height showed deviations from linearity for larger particles (100 nm AuNPs), it demonstrated greater accuracy (lower bias) for smaller NPs (20 nm and 30 nm), indicating its potential to improve the LoQ in SP-ICP-MS.

Furthermore, peak height proved valuable in setting appropriate threshold values, as integrated intensity is more susceptible to bias, particularly in complex sample matrices where threshold selection is less straightforward. Additionally, the monitoring of peak height can significantly improve the estimation of the LoD in SP-ICP-MS, providing a more realistic value, not hampered by geometrical assumptions.

Overall, peak height should not be overlooked and deserves further investigation as a complementary or alternative signal to enhance the quality of SP-ICP-MS results, and of single-event ICP-MS in general.

CRediT authorship contribution statement

Antonio Bazo: Writing – original draft, Validation, Software, Methodology, Investigation, Formal analysis, Data curation, Conceptualization. **Lorién López-Villellas:** Software. **Matilde Mataloni:** Formal analysis, Data curation. **Eduardo Bolea-Fernandez:** Writing – review & editing, Visualization, Conceptualization. **Ana Rua-Ibarz:** Writing – review & editing, Visualization, Supervision, Conceptualization. **Marco Grotti:** Supervision. **Maite Aramendía:** Writing – review & editing, Visualization, Supervision. **Martín Resano:** Writing – review & editing, Supervision, Resources, Project administration, Funding acquisition.

Declaration of competing interest

The authors declare that they have no known competing financial interests or personal relationships that could have appeared to influence the work reported in this paper.

Acknowledgements

The authors are grateful to the European Regional Development Fund ("ERDF A way of making Europe") for financial support through the Interreg POCTEFA Nanolyme EFA99/1, to project PID2021-122455NB-I00 (funded by MCIN/AEI/10.13039/501100011033 and by ERDF) and also to the Aragon Government (DGA: Grupo E43_20R and grant PROY_E17_24). A.B. acknowledges the Department of Science, University and Knowledge Society from DGA his predoctoral grant (2021 call). L.L.-V. acknowledges the Department of Science, University and Knowledge Society from DGA his predoctoral grant (2022 call), the Spanish Ministry of Science and Innovation MCIN/AEI/10.13039/501100011033 (grant PID2022-136454NB-C22), and the Government of Aragon (T58_23R research group). M.M. acknowledges the University of Genoa and the MUR for her predoctoral grant (2023 call). E.B.-F. acknowledges financial support from the Ramón y Cajal programme (RYC2021-031093-I) funded by MCIN/AEI/10.13039/501100011033 and the European Union (NextGenerationEU/PRTR). A.R.-I. thanks European Union's Horizon 2020 research and innovation program under the Marie-Sklodowska-Curie grant agreement N° 101034288.

Data availability

Data will be available through Zenodo.

References

[1] J. Vidmar, R. Milačič, J. Ščančar, Sizing and simultaneous quantification of nanoscale titanium dioxide and a dissolved titanium form by single particle inductively coupled plasma mass spectrometry, Microchem. J. 132 (2017) 391–400, https://doi.org/10.1016/j.microc.2017.02.030.

[2] M.E. Johnson, S.K. Hanna, A.R. Montoro Bustos, C.M. Sims, L.C.C. Elliott, A. Lingayat, A.C. Johnston, B. Nikoobakht, J.T. Elliott, R.D. Holbrook, K.C.K. Scott, K.E. Murphy, E.J. Petersen, L.L. Yu, B.C. Nelson, Separation, sizing, and quantitation of engineered nanoparticles in an organism model using inductively coupled plasma mass spectrometry and image analysis, ACS Nano 11 (2017) 526–540, https://doi.org/10.1021/acsnano.6b06582.

[3] R. Gonzalez de Vega, T.E. Lockwood, X. Xu, C. Gonzalez de Vega, J. Scholz, M. Horstmann, P.A. Doble, D. Clases, Analysis of Ti- and Pb-based particles in the aqueous environment of Melbourne (Australia) via single particle ICP-MS, Anal. Bioanal. Chem. 414 (2022) 5671–5681, https://doi.org/10.1007/s00216-022-04052-0.

[4] J. Vidmar, L. Hässmann, K. Loeschner, Single-particle ICP–MS as a screening technique for the presence of potential inorganic nanoparticles in food, J. Agric. Food Chem. 69 (2021) 9979–9990, https://doi.org/10.1021/acs.jafc.0c07363.

[5] E. Espada-Bernabé, B. Gómez-Gómez, G. Moreno-Martín, Y. Madrid, Development of a fast and low-cost aqueous based-extraction protocol for the simultaneous extraction and characterization of SiO2 and TiO2 (nano)particles in confectionary products, Anal. Chim. Acta 1323 (2024) 343058, https://doi.org/10.1016/j.aca.2024.343058.

[6] E. Espada-Bernabé, G. Moreno-Martín, B. Gómez-Gómez, Y. Madrid, *In Vitro* gastrointestinal stability and Caco-2 cell cytotoxicity of TiO2 and SiO2 (nano) particles from confectionary products, Food Res. Int. 202 (2025) 115754, https://doi.org/10.1016/j.foodres.2025.115754.

[7] S. Fernández-Trujillo, M. Jiménez-Moreno, Á. Ríos, R. Martín-Doimeadios, A simple analytical methodology for platinum nanoparticles control in complex clinical matrices via SP-ICP-MS, Talanta 231 (2021) 122370, https://doi.org/10.1016/j.talanta.2021.122370.

[8] R. Zhao, J. Xiang, B. Wang, L. Chen, S. Tan, Recent advances in the development of noble metal NPs for cancer therapy, Bioinorgan. Chem. Appl. 2022 (2022) 2444516, https://doi.org/10.1155/2022/2444516.

[9] D. Mozhayeva, C. Engelhard, A critical review of single particle inductively coupled plasma mass spectrometry – a step towards an ideal method for nanomaterial characterization, J. Anal. At. Spectrom. 35 (2020) 1740–1783, https://doi.org/10.1039/C9JA00206E.

[10] M. Resano, M. Aramendía, E. García-Ruiz, A. Bazo, E. Bolea-Fernandez, F. Vanhaecke, Living in a transient world: ICP-MS reinvented via time-resolved analysis for monitoring single events, Chem. Sci. 13 (2022) 4436–4473, https://doi.org/10.1039/D1SC05452J.

[11] C. Degueldre, P.-Y. Favarger, Colloid analysis by single particle inductively coupled plasma-mass spectroscopy: a feasibility study, Colloids Surf. A Physicochem. Eng. Asp. 217 (2003) 137–142, https://doi.org/10.1016/S0927-7757(02)00568-X.

[12] H.E. Pace, N.J. Rogers, C. Jarolimek, V.A. Coleman, C.P. Higgins, J.F. Ranville, Determining transport efficiency for the purpose of counting and sizing nanoparticles via single particle inductively coupled plasma mass spectrometry, Anal. Chem. 83 (2011) 9361–9369, https://doi.org/10.1021/ac201952t.

[13] S. Cuello-Nuñez, I. Abad-Álvaro, D. Bartczak, M.E. del C. Busto, D.A. Ramsay, F. Pellegrino, H. Goenaga-Infante, The accurate determination of number concentration of inorganic nanoparticles using spICP-MS with the dynamic mass flow approach, J. Anal. At. Spectrom. 35 (2020) 1832–1839, https://doi.org/10.1039/C9JA00415G.

[14] B. Moreira-Álvarez, L. Cid-Barrio, F. Calderón-Celis, J.M. Costa-Fernández, J. R. Encinar, Relative and transport efficiency-independent approach for the determination of nanoparticle size using single-particle ICP-MS, Anal. Chem. 95 (2023) 10430–10437, https://doi.org/10.1021/acs.analchem.3c01823.

[15] M.I. Chronakis, B. Meermann, M. von der Au, The evolution of data treatment tools in single-particle and single-cell ICP-MS analytics, Anal. Bioanal. Chem. 417 (2025) 7–13, https://doi.org/10.1007/s00216-024-05513-4.

[16] B. Meermann, V. Nischwitz, ICP-MS for the analysis at the nanoscale – a tutorial review, J. Anal. At. Spectrom. 33 (2018) 1432–1468, https://doi.org/10.1039/C8JA00037A.

[17] A.M. Duffin, E.D. Hoegg, R.I. Sumner, T. Cell, G.C. Eiden, L.S. Wood, Temporal analysis of ion arrival for particle quantification, J. Anal. At. Spectrom. 36 (2021) 133–141, https://doi.org/10.1039/D0JA00412J.

[18] A. Schardt, J. Schmitt, C. Engelhard, Single particle inductively coupled plasma mass spectrometry with nanosecond time resolution, J. Anal. At. Spectrom. 39 (2024) 389–400, https://doi.org/10.1039/D3JA00373F.

[19] A. Kéri, I. Kálomista, D. Ungor, Á. Bélteki, E. Csapó, I. Dékány, T. Prohaska, G. Galbács, Determination of the structure and composition of Au-Ag bimetallic spherical nanoparticles using single particle ICP-MS measurements performed with normal and high temporal resolution, Talanta 179 (2018) 193–199, https://doi.org/10.1016/j.talanta.2017.10.056.

[20] A. Bazo, E. Bolea-Fernandez, A. Rua-Ibarz, M. Aramendía, M. Resano, Intensity- and time-based strategies for micro/nano-sizing *via* single-particle ICP-mass spectrometry: a comparative assessment using Au and SiO2 as model particles, Anal. Chim. Acta 1331 (2024) 343305, https://doi.org/10.1016/j.aca.2024.343305.

[21] I. Kálomista, A. Kéri, D. Ungor, E. Csapó, I. Dékány, T. Prohaska, G. Galbács, Dimensional characterization of gold nanorods by combining millisecond and microsecond temporal resolution single particle ICP-MS measurements, J. Anal. At. Spectrom. 32 (2017) 2455–2462, https://doi.org/10.1039/C7JA00306D.

[22] J. Liu, X. Wei, C. Wu, L. Zheng, M. Wang, M. Chen, J. Wang, Data analysis for the characterization of nanoparticles with single particle inductively coupled plasma mass spectrometry: from microsecond to millisecond dwell times, Anal. Chim. Acta 1254 (2023) 341114, https://doi.org/10.1016/j.aca.2023.341114.

[23] A.F. Kadjo, P.K. Dasgupta, J. Su, S. Liu, K.G. Kraiczek, Width based quantitation of chromatographic peaks: principles and principal characteristics, Anal. Chem. 89 (2017) 3884–3892, https://doi.org/10.1021/acs.analchem.6b04857.
[24] F.V. Nakadi, M.A.M.S. da Veiga, M. Aramendía, E. García-Ruiz, M. Resano, Chlorine isotope determination via the monitoring of the AlCl molecule by high-resolution continuum source graphite furnace molecular absorption spectrometry – a case study, J. Anal. At. Spectrom. 30 (2015) 1531–1540, https://doi.org/10.1039/C5JA00055F.
[25] A. Bazo, R. Garde, E. Garcia-Ruiz, M. Aramendía, F.V. Nakadi, M. Resano, High-resolution continuum source graphite furnace molecular absorption spectrometry for the monitoring of Sr isotopes via SrF formation: a case study, J. Anal. At. Spectrom. 37 (2022) 2517–2528, https://doi.org/10.1039/D2JA00245K.
[26] N. Dyson, Chromatographic Integration Methods, Royal Society of Chemistry, 1998.
[27] J. Tuoriniemi, G. Cornelis, M. Hassellöv, A new peak recognition algorithm for detection of ultra-small nano-particles by single particle ICP-MS using rapid time resolved data acquisition on a sector-field mass spectrometer, J. Anal. At. Spectrom. 30 (2015) 1723–1729, https://doi.org/10.1039/C5JA00113G.
[28] T.E. Lockwood, R.G. de Vega, D. Clases, An interactive Python-based data processing platform for single particle and single cell ICP-MS, J. Anal. At. Spectrom. 36 (2021) 2536–2544, https://doi.org/10.1039/D1JA00297J.
[29] M. Aramendía, J.C. García-Mesa, E.V. Alonso, R. Garde, A. Bazo, J. Resano, M. Resano, A novel approach for adapting the standard addition method to single particle-ICP-MS for the accurate determination of NP size and number concentration in complex matrices, Anal. Chim. Acta 1205 (2022) 339738, https://doi.org/10.1016/j.aca.2022.339738.
[30] F. Laborda, A.C. Gimenez-Ingalaturre, E. Bolea, J.R. Castillo, About detectability and limits of detection in single particle inductively coupled plasma mass spectrometry, Spectrochim. Acta B Atom Spectrosc. 169 (2020) 105883, https://doi.org/10.1016/j.sab.2020.105883.
[31] M.D. Montaño, J.W. Olesik, A.G. Barber, K. Challis, J.F. Ranville, Single particle ICP-MS: advances toward routine analysis of nanomaterials, Anal. Bioanal. Chem. 408 (2016) 5053–5074, https://doi.org/10.1007/s00216-016-9676-8.
[32] J. Navratilova, A. Praetorius, A. Gondikas, W. Fabienke, F. von der Kammer, T. Hofmann, Detection of engineered copper nanoparticles in soil using single particle ICP-MS, Int. J. Environ. Res. Publ. Health 12 (2015) 15756–15768, https://doi.org/10.3390/ijerph121215020.
[33] A. Bazo, E. Bolea-Fernandez, A. Rua-Ibarz, M. Aramendía, M. Resano, Ions with ions, entities with entities: a proof-of-concept study using the SELM-1 yeast certified reference material for Intra- and extracellular Se quantification via single-cell ICP-mass spectrometry, Anal. Chem. 97 (2025) 13922–13929, https://doi.org/10.1021/acs.analchem.5c01588.